High-Fidelity Simulations of Blast Loadings in Urban Environments Using an Overset Meshing Strategy

Xiao Wang[1], Michael Remotigue[2], Qiuhan Arnoldus[1], Mark Janus[3], Edward Luke[4],

David Thompson[3], Richard Weed[1] , and Gregory Bessette[5]

Affiliation

[1]Center for Advanced Vehicular Systems (CAVS)

[2]Center for Advanced Vehicular Systems (currently with Pointwise, Inc.)

[3]Department of Aerospace Engineering

[4]Department of Computer Science and Engineering

Mississippi State University

Mississippi State, MS 39762, USA

[5]US Army Engineer Research and Development Center, Geotechnical and Structures

Laboratory, Vicksburg, MS 39180, USA

ABSTRACT

Detailed blast propagation and evolution through multiple structures representing an urban environment were simulated using the code *Loci/BLAST*, which employs an overset meshing strategy. The use of overset meshes simplifies mesh generation by allowing meshes for individual component geometries to be generated independently. Detailed blast propagation and evolution through multiple structures, wave reflection and interaction between structures, and blast loadings on structures were simulated and analyzed. Predicted results showed good agreement with experimental data generated by the US Army Engineer Research and

Development Center. *Loci/BLAST* results were also found to compare favorably to simulations obtained using the Second-Order Hydrodynamic Automatic Mesh Refinement Code (SHAMRC). The results obtained demonstrated that blast reflections in an urban setting significantly increased the blast loads on adjacent buildings. Correlations of computational results with experimental data yielded valuable insights into the physics of blast propagation, reflection, and interaction under an urban setting and verified the use of *Loci/BLAST* as a viable tool for urban blast analysis.

KEYWORDS: Blast, Urban Environment, Multiple Structures, Simulation, Overset Mesh.

1. INTRODUCTION

Blasts in urban environments, whether intentional or accidental in origin, typically result in serious injury and loss of life as well as extensive property damage. A contributing factor is the urban environment itself due to the interaction of the blast wave with multiple nearby structures, which could have a significant effect on the resulting blast loading on all of the buildings in the path of the blast wave. Due to the blast reflections and interactions, it is possible to markedly increase the loading on an affected structure that is in close proximity to other structures relative to the loading on the same structure in isolation. Analytically- and empirically-based software packages that can be used to predict blast loadings have the advantage of being computationally efficient. However, these tools may not accurately account for interference effects. In contrast, high-fidelity physics-based numerical simulations, while more accurate, require a substantial investment in computational resources.

For high-fidelity blast simulations that employ body-fitted meshes, generating the needed meshes, especially for problem containing multiple structures, can be a time-consuming task. These difficulties are primarily associated with the requirements placed on the underlying geometric description. Additionally, if the geometry is modified, the mesh must be regenerated.

The necessary geometry and mesh generation processes require significant expertise and, in some cases, a relatively high level of user sophistication.

This paper describes a newly-developed, high-fidelity strategy for simulating blast effects in an urban environment. The code used to simulate the blast was *Loci*/*BLAST* [1-4], which utilizes body-fitted, component-based, overset meshes to simplify the geometry modeling and mesh generation aspects of the problem. In an overset meshing paradigm [5], a mesh appropriate for each geometrical component is generated independently from all other components. These component meshes are then embedded in a background mesh and communication between the various meshes is performed using interpolation. The overset mesh technique not only simplifies initial meshing requirements, it also facilitates the simulation of problems involving dynamic motion such as would be involved in debris tracking. One goal of this paper is to evaluate the accuracy impact of using overset techniques in blast problems.

Validation of *Loci/BLAST* for blast in urban environments was performed by comparing predicted results to experimental data obtained by the US Army Engineer Research and Development Center (ERDC) and to results predicted by the Second-Order Hydrodynamic Automatic Mesh Refinement Code (*SHAMRC*) [6]. ERDC conducted a combined experimental/numerical study on blast in urban terrain. In these small-scale experiments, blast propagation in a notional urban environment was investigated. Simulations were also performed using *SHAMRC* to study air blast loads on the tested structures.

2. LITERATURE REVIEW

Over the past 20 years, many HPC-based codes have been developed or extended to support the analysis of blast effects on structures. Those codes usually fall into one of two categories,

either Eulerian shock-physics codes (e.g., see [7-9]) or Lagrangian/Arbitrary Lagrangian-Eulerian (ALE) finite-element codes (e.g., see [10, 11]).

A numerical simulation based on the Eulerian formulation of the governing equations computes the flow field on a fixed mesh that allows the fluid to pass through it. Eulerian codes can simulate blast-structure interactions with high fidelity. Several codes of this type have been developed and extensively used to study blast loading on structures. *CTH* [12] is a shock-physics code that models multi-material flows of solids and liquids under high pressure and high strain rates. It includes several different equations of state (EoS) for energetic materials as well as programmed and reactive burn models for the detonation process. It supports dynamic Adaptive Mesh Refinement (AMR) and includes full constitutive models for material strength including elastic-plastic flows. However, *CTH* does not treat afterburn and is thus not appropriate for explosions in confined regions involving oxygen deficient explosives. *SHARC*/*SHAMRC* [13] employs a finite-difference, operator-split algorithm and a Cartesian grid system. Unlike *CTH*, it does not support analysis of solids with full material strength. A mixing-controlled afterburn model is available in its recent versions. *FEFLO* [14] has been applied to a variety of air blast problems including urban blast [15]. A relatively crude afterburn model was added recently [16]. *SAGE* [17] was originally developed as a multi-material water-shock code, but has also been used extensively for air blast and gaseous explosions. *SAGE* contains a mixing-controlled afterburn model and also supports a robust and reliable AMR. *MAZ* (Multiphase Adaptive Zoning) has been applied to air blast in an urban environment [18]. *Chinook* has combustion and afterburn capabilities including burning of aluminum particles. It treats group Lagrange particles, multiphase flow, and multiple materials [19].

In contrast, Lagrangian methods utilize a mesh that moves with the material components and allows simulation over long time scales. *AUTODYN* [20] was originally developed as a finite-element code for impact analysis. It was extended to include Eulerian and ALE finite-

volume schemes for Fluid-Structure Interacting (FSI) and applied to a variety of blast problems [21]. *ALE3D* [22] can model a wide range of multi-material flow problems. It has demonstrated capabilities for blast problems that are similar to both *CTH* and *SHAMRC*. *LS-DYNA* [23] is a finite-element code originally developed for structural dynamics problems. Recent extensions to *LS-DYNA* include an ALE capability for modeling multi-material FSI and a "LOAD_BLAST" capability that uses a zeroth-order model based on *CONWEP* [24] to compute loads on structures due to blast. These new capabilities have led to increased use of *LS-DYNA* for blast analysis.

However, both Eulerian and Lagrangian methods have limitations in simulating blast effects. Eulerian methods are often limited to a relatively short simulation time span. Lagrangian methods are not able to accurately simulate complex structural interactions and reflected pressure waves, especially in regions near the detonation. Therefore, it becomes necessary to leverage the strengths of both the Eulerian and Lagrangian approaches by coupling an Eulerian shock-physics code with a Lagrangian structural dynamics code. The *ZAPOTEC* code [25], which couples *CTH* with the *PRONTO3D* finite-element code, has been used for a variety of blast problems including contact detonation on reinforced concrete structures. *DYSMAS* couples *GEMINI*, an operator-split hydrocode, with the Navy's version of the *DYNA2D* structural analysis code. *DYSMAS* has now been linked with *PARADYN*, which is a parallel version of *DYNA3D*. *DYSMAS* has been applied to the design of blast barriers [26]. Other examples of this type include couplings of *Chinook* code with *LS-DYNA*, and *FEFLO* with *DYNA3D*. In fact, the blast code used in this research, *Loci/BLAST*, has been coupled with *LS-DYNA* to model the structural effects of blast on vehicles [2-4].

3. BLAST MODELING

The numerical methods employed in *Loci/BLAST* are described in detail in Thompson *et al*. [1-3] and Invancic *et al*. [4]. *Loci/BLAST* is a relatively new blast code that extends the

5

capabilities of the *Loci/CHEM* flow solver [27] to model blast events through the addition of advanced equations of state (EoS), such as the Jones-Wilkins-Lee (JWL) EoS [28]. *Loci/BLAST* has also been used to simulate detailed blast-soil interactions [2]. *Loci/CHEM* is a full-featured flow solver that has undergone extensive verification and validation and has been demonstrated to scale efficiently to thousands of processors [29].

3.1 Governing Equations

The governing equations for the blast model are those of a multicomponent inviscid flow assuming thermal, pressure, and velocity equilibrium between all materials in any given region in space. These equations are described by the conservation of component mass, momentum, and energy, which are given by

$$\frac{\partial \rho_i}{\partial t} + \nabla \bullet (\rho_i \vec{u}) = 0, \forall i \in \{1 \dots NS\} \tag{1}$$

$$\frac{\partial \rho \vec{u}}{\partial t} + \nabla \bullet (\rho \vec{u} \vec{u}) = \nabla p \tag{2}$$

$$\frac{\partial \rho e_0}{\partial t} + \nabla \bullet [(\rho e_0 + p)\vec{u}] = 0 \tag{3}$$

Here, ρ_i is the component density of material i, $\vec{u}$ is the material velocity vector, p is the pressure of the component mixture. Note that *NS* is the number of component species and the overall material density at any point is given by $\rho = \Sigma_{i=1}^{NS} \rho_i$. The total energy per unit mass, e_0, is the sum of the fluid kinetic energy and internal energy given by the expression

$$e_0 = \frac{1}{2} \vec{u} \cdot \vec{u} + e_{internal} \tag{4}$$

These equations are closed by a multicomponent EoS that relates pressure to the material densities of the components and the internal energy as represented by $p = p(\rho_1, \rho_2, \cdots, \rho_{NS}, e_{internal})$. The formulation of this EoS is central to the soil and blast gas models, which are derived from

a mixture rule that combines single component equations of state for each material, assuming pressure and thermal equilibrium.

3.2 Multicomponent EoS for Blast Modeling

To support non-ideal equations of state for blast modelling, a robust density-energy query capability is needed. The resulting mixing rule assumes that the materials are immiscible and are in mechanical (pressure) and thermal equilibrium. In this mixing rule, it is assumed that the mixture of species equations of state which define pressure as a function of density and temperature. Using the immiscible assumption, we find the volume of the mixture is the sum of the volume occupied by each species, or

$$\frac{1}{\rho} = \sum_{i=1}^{NS} \frac{Y_i}{\rho_i^*} \tag{5}$$

where Y_i is the species mass fraction and ρ_i^* is the density of a pure material i at a given temperature and pressure as given by

$$p = p_i\left(\rho_i^*, T\right) \forall \ i \in [1 \dots NS] \tag{6}$$

where $p_i\left(\rho_i^*, T\right)$ is the EoS for species i, and p is the system pressure. The energy of the mixture is given by the mass averaged species energies, as in

$$e = \sum_{i=1}^{NS} Y_i e_i\left(T, \rho_i^*\right) \tag{7}$$

where the species energy equation is given by

$$e_i\left(T, \rho_i^*\right) = e_{f,i} + \int_{T_o}^{T} c_{v,i}(\tau)d\tau + \left[e_i\left(T, \rho_i^*\right) - e_i(T)_{pg}\right] \tag{8}$$

The last term in this expression is a departure function that accounts for the effects of non-ideality in the EoS. Note that equation (8) is simply a trivial regrouping of the energy components that allows us to view the energy of a species as a division of thermally perfect and thermally

7

imperfect components. Thus the departure function is viewed as the deviation of the energy equation from a thermally perfect gas and can be computed using

$$\left[e_i\left(T, \rho_i^*\right) - e_i\left(T\right)_{pg} \right] = \int_0^{\rho_i^*} \left[p - T \frac{\partial p\left(\rho_i^*, T\right)}{\partial T} \right] \frac{d\rho_i^*}{\rho_i^{*2}} \tag{9}$$

Equations (5), (6), and (7) describe $NS+2$ nonlinear equations and $NS+4$ unknowns (the unknowns are the species specific volumes $1/\rho_i^*$ and the thermodynamic variables P, T, ρ, and e). Given any two thermodynamic state variables, this system of equations can be solved to find the remaining thermodynamic variables along with the specific volumes implied by the species pure substance densities ρ_i^*. Due to the inherent non-linearities in these equations, robustly solving for the thermodynamic state, given the fluid density and energy (as will be required by an explicit time integrator), can be a significant challenge. The most straightforward approach is to use a multi-dimensional Newton method. However, when the initial guess is far away from the final solution, it can be difficult to converge reliably to a solution. We have developed an alternative approach that is robust, but perhaps with a sacrifice in computational efficiency.

To obtain a robust solution to the above non-linear equations, it can be observed that if the problem is cast in terms of pressure and temperature instead of density and energy, the pressure equation, i.e., equation (6), decouples and NS non-linear scalar equations must be solved. Since non-linear root finding for scalar equations can be made robust using root bracketing techniques, the pressure-temperature query has a very robust solution. This observation can be used to implement an indirect procedure that provides a robust density-energy EoS query. First, a robust density-temperature query can be obtained by performing a bracketed-scalar solve for the pressure. This iterative solve can utilize the robust pressure-temperature query; in addition, it is expected that pressure will increase monotonically with temperature. Finally, given a robust density-temperature query, a robust density-energy query can be formulated by solving for the temperature that gives the specified energy. All of these queries are solved using a bracketed

8

Newton method whereby the values that bracket a solution are identified. If the Newton method overshoots the bracket, the robust bisection method is utilized for that step. The resulting EoS query evaluator has been shown to be robust in practice. A variety of species equations of state have been implemented in *Loci/BLAST* including a perfect gas, a density-temperature form of the JWL EoS for the explosive gas [28], a linear barytropic EoS for an elastic solid (explosive and soil), and a Tait EoS for liquid water [30].

Note that unlike *Loci/BLAST*, many Lagrangian remap based hydrocodes such as CTH do not establish mixture thermal and mechanical equilibration at every timestep with respect to their treatment of mixture EoS and instead use techniques that will converge to an equilibrium result provided that meshes and timesteps are appropriately refined. While it is true that our EoS evaluation is more expensive than these non-equilibrium approaches, we have observed that *Loci/BLAST* will frequently achieve mesh independence at a coarser mesh (and timestep) than comparable hydrocodes and we attribute this to the fact that we obtain thermodynamic equilibrium within each timestep. This tradeoff of computational expense of a timestep versus the productivity of the timestep is difficult to quantify without more careful study than has been conducted so far, but the difference in mesh sizes required to obtain mesh independent solutions appears to be significant and could easily make up the difference in cost for three dimensional computations.

3.3   Prescribed Burn Model

A prescribed burn capability is used to simulate the propagation of the detonation front through the explosive material. The current model assumes that the detonation is initiated from a single point and that there are no obstructions to the detonation front. In the prescribed explosive burn methodology, the initiation point and a detonation velocity are provided by the user. The explosive burn is accomplished by converting the solid explosive material into the corresponding gas material as the detonation wave passes each given point in the mesh. Usually the solid

explosive before detonation is modeled as an elastic solid, while gasses released by the burn are modeled using the JWL EoS [31]. To accomplish the appropriate energy release during the burn, the heat of formation of the solid explosive material is set such that the proper heat release is achieved.

The detonation front is computed by enforcing a burn fraction that is a function of the lighting time, t_1. The lighting time is the computed time that the detonation front will arrive at a given cell and is computed by dividing the distance to the initiation point by the detonation velocity, D. The burn fraction, F, is zero if $t \leq t_1$. When $t > t_1$, the burn fraction is defined by

$$F = \max\left(\frac{(t - t_1)D}{4\Delta}, \frac{1-V}{1-V_{CJ}} \right) \tag{10}$$

where t is the current simulation time, t_1 is the current cell lighting time, D is the detonation velocity, $V = \rho_0/\rho$ is the relative volume, V_{CJ} is the relative volume at the Chapman-Jouguet conditions, and Δ is an estimated grid spacing for the mesh where the detonation front is propagating.

3.4   Numerical Considerations

When simulating multicomponent flows, it is possible to take a time-step such that the material in a cell is completely depleted, resulting in the time evolution of negative mass fractions of material. This non-physical circumstance is unacceptable because advancing the solution becomes nearly impossible. For first-order spatial approximations, depletion of the material from a cell is avoided if a time-step is employed that satisfies the stable CFL (Courant-Friedrichs-Lewy) condition. However, when reconstructing higher-order mixture fractions, it is possible to deplete a material even though a much smaller time-step is used. To facilitate a second-order spatial reconstruction of species mass fractions, the mass fraction extrapolation is limited to ensure that a negative mass fraction is avoided (assuming a first-order upwind

convection). While such limiting helps avoid the evolution of negative mass fractions, they can still occur. Therefore, to provide an effective strategy that avoids negative mass fraction evolution in the time-stepping algorithm, the time-step is further limited to include the time required to deplete a cell of all species material using the first time-step residual. In practice, a CFL between 0.5 and 0.75 may still be required to avoid the evolution of negative mass fractions.

For the solution of the inviscid equations, the positivity-preserving HLLE (Harten, Lax, van Leer and Einfeldt) flux proposed by Einfeldt [32] is utilized. Second-order reconstructions are provided by utilizing primitive variable reconstructions of pressure, temperature and velocity with limiting provided by the multi-dimensional limiter of Barth and Jespersen [33] applied to the cell nodal extrapolations. The inviscid fluxes were then integrated in time using a second-order, two-step, explicit Runge-Kutta integrator that satisfies the TVD (total-variation-diminishing) conditions [34]. Mass source terms provided by the prescribed burn model were computed using a Strang operator splitting method.

4. OVERSET MESHING STRATEGY

The task of generating body-fitted meshes for an urban environment consisting of multiple nearby structures can require a high level of time-consuming user interaction. To address this issue, an overset meshing strategy was employed [5]. In an overset-mesh framework, component meshes for individual objects are created without regard to neighboring objects. In this case, all-tetrahedron meshes were employed for each of the component meshes. The component meshes were then embedded in a Cartesian background mesh, which represents the basic topography of the landscape and the remainder of the computational domain. The cityscape is then formed by overlaying component meshes of individual buildings onto the background mesh. The background mesh is then refined to improve the quality of the

11

interpolation between the background mesh and the component meshes [35]. In this context, refinement occurs in areas in close proximity to the buildings and the charge. Refinement reduces the memory requirements and computational cost by allowing a very coarse mesh in the far field. The optimized background mesh is then merged with the component meshes.

One challenge presented in the creation of overset meshes is the need to remove mesh elements from one mesh where it overlaps with another mesh. A removal process known as hole cutting is needed. The hole-cutting approach developed in this work utilized a medial surface that is similar to that employed by Togashi *et al.* [36]. In the automated hole-cutting algorithm, each component mesh has a simple external surface that defines the region of its application. If two regions overlap, then the region is assigned to the component or background mesh that contains a surface that is closest. As a result, the hole cutting is defined by a combination of the outer surface of the component analytic geometry and the medial surface that is formed between the surfaces of each component mesh.

The entire meshing process, including defining geometry and domain, generating component meshes, background mesh refinement, merge of component and background mesh, automatic hole cutting, was performed with a set of highly automatic in-house developed tools, which allows users to quickly place structures on existing topography to evaluate different design scenarios.

Simulations reported in Section 5 focus on two different configurations (Figure 1) for which experimental data were available. For a two-building case, a C4 charge was placed on the centerline in front of two structures as depicted in Figure 1, where five probes at representative locations were marked as well for data recording. For a one-building case, only the charge and the small building were included. The small structure was placed 205 mm away from the center of explosives, and its dimensions were 336 mm $\times$ 336 mm $\times$ 458 mm. The large structure was 846 mm away from the center of the charge, and its dimensions were 572

mm $\times$ 572 mm $\times$ 737 mm. These configurations will be employed in the discussion below to illustrate the overset meshing strategy.
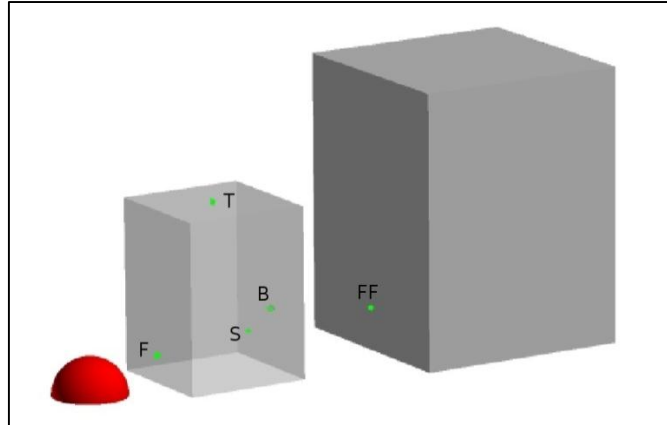
Figure 1. Case setup: C4 charge (red), two buildings and probes (green)

To assure mesh independence and consistence between the overset and single meshes, a series test simulations were conducted regarding issues of computational domain, mesh resolution and refinement. In a test run of the one-building case on a single mesh of the hemisphere domain with a radius of 2.1 times the height of the structure, outer boundary unphysical wave reflections were observed. Such wave reflection was avoided in a further test on an extended domain, where its radius was 5.25 times the height of the structure. In a refinement process for overset mesh, the coarsening of local grid spacing is controlled by a power law as a function of the distance to considered features, where larger value of exponent implies faster coarsening of the background mesh. Locations and geometries of the charge and the buildings are considered the features of interest. Test meshes were generated with exponents of 1.0 (linear), and 1.5 (super linear) for the one-building case, which yielded a fine mesh of 14.26 million cells, and a coarse mesh of 9.90 million cells, respectively. For comparison purpose, a single mesh of 18.41 million cells was also generated. Resolved blast waves recorded at probe F (as noted in Figure 1) on the single mesh and the fine overset mesh showed good agreement in Figure 2, in terms of peak pressures, arrival time, and impulse shapes. The peak pressure

obtained on the fine overset mesh is 4.5% higher than what simulated on the single mesh.

Results simulated on the coarse mesh indicated that a slight super linear (exponent 1.5)

coarsening of the background mesh degraded the accuracy of wave capture. Therefore, a

meshing strategy using linear coarsening in the refinement process was adopted in the overset

mesh generation in this work.
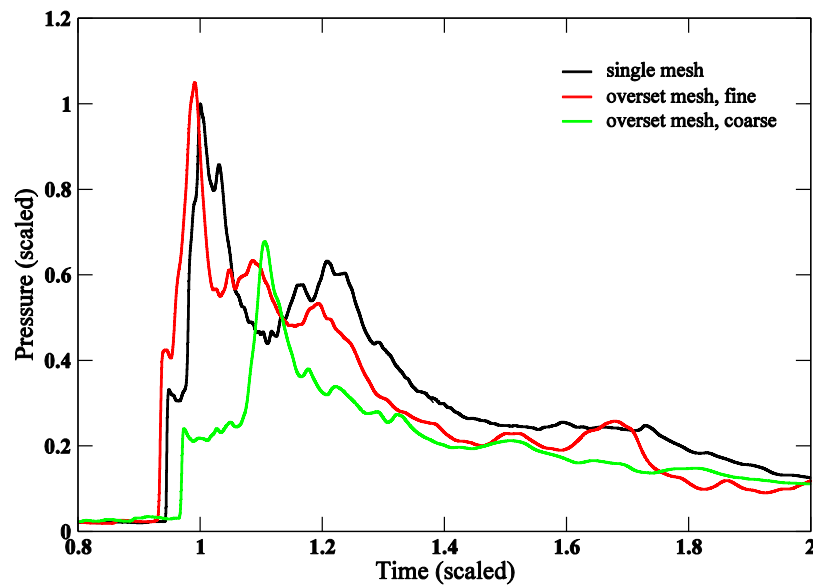
Figure 2. Comparison of resolved blast waves on different meshes

Based on the meshing strategy obtained from the mesh study, two overset meshes were

generated for the one-building case and the two-building case, respectively (Figure 3). A close-

up view shows a gradual change in mesh spacing around the multiple structures. Grid spacings

of 1.0 mm in the charge region, 3.0 mm on structures, and 1.0 cm on the outer boundaries of

building components were specified in both cases. The outer boundaries were positioned far

enough away from the structures and charge to avoid non-physical wave reflections. In the one-

building mesh, distances between any domain outer boundary and structure surfaces are larger

than 4.2 times the height of the small building. This distance was extended to 5.0 times the

height of the small building in the two-building mesh. In the two-building mesh, the larger

structure was introduced downstream the small structure and the domain was extended, which

increased mesh size dramatically. The resultant two-building mesh had 62.27 million cells, while the one-building mesh had 14.26 million cells.

In order to verify the consistency between blast simulations on the overset-mesh and single-mesh computational domains, simulations were performed on all-tetrahedron single-mesh grids (Figure 4) as well. The single-mesh domain is a hemisphere above the ground with the charge positioned in the center. The radius of the domain was 5.5 times the height of the small structure for the one-building case, and 8.7 for the two-building case. In the one-building mesh, grid spacings of 1.8 mm and 10 cm were defined on the structure, and the outer boundary, respectively. In the two-building mesh, grid spacings on structures were slightly relaxed to 3 mm. The resultant two-building grid contained 47.44 million cells, and the one-building grid had 18.41 million cells. To display and compare meshes and computational domains, a cutting plane through the centerline of buildings and charge was extracted from each grid and viewed at the same zoom and scale in Figures 3 and 4. Buildings were outlined by green lines and charge's conceptualized radius was indicated by a red semicircle.
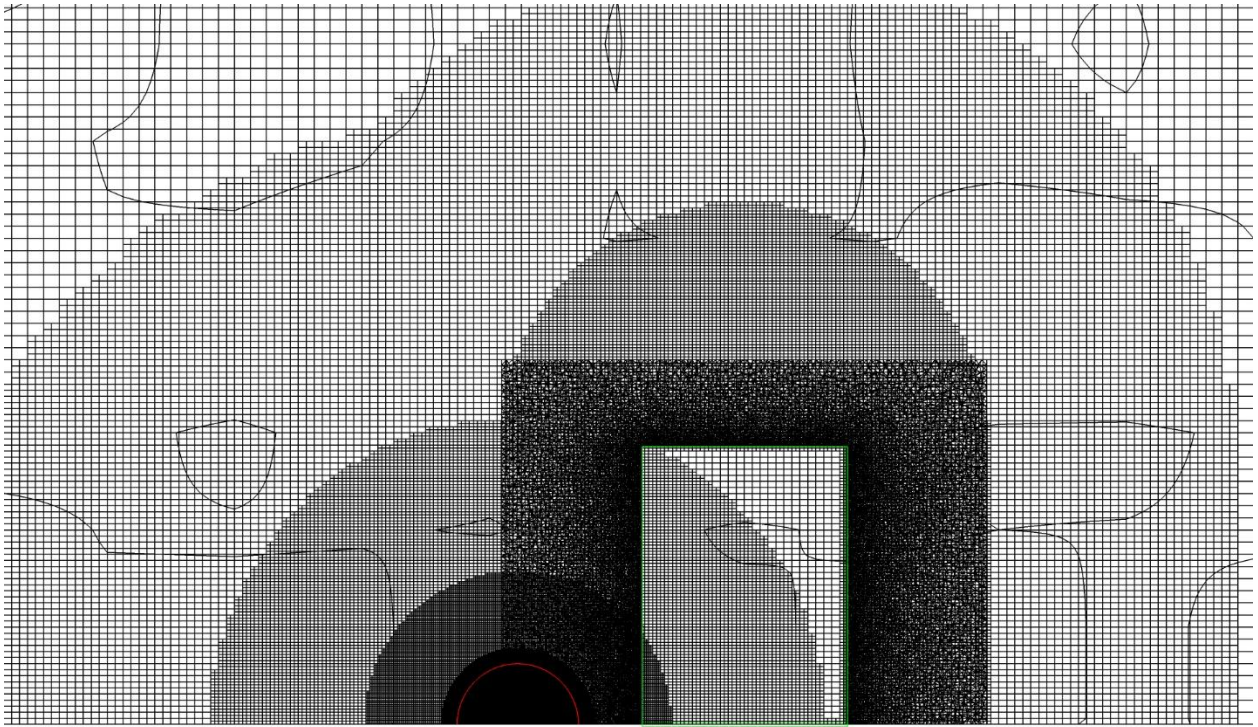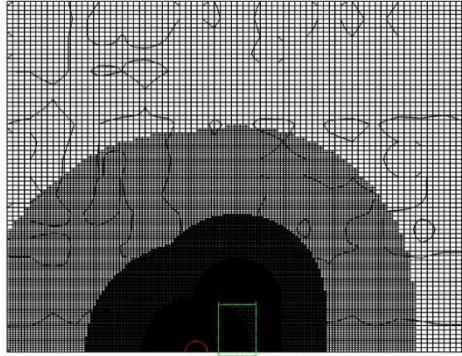
(a) Single-building overset mesh, full view (above) and close-up view (below)
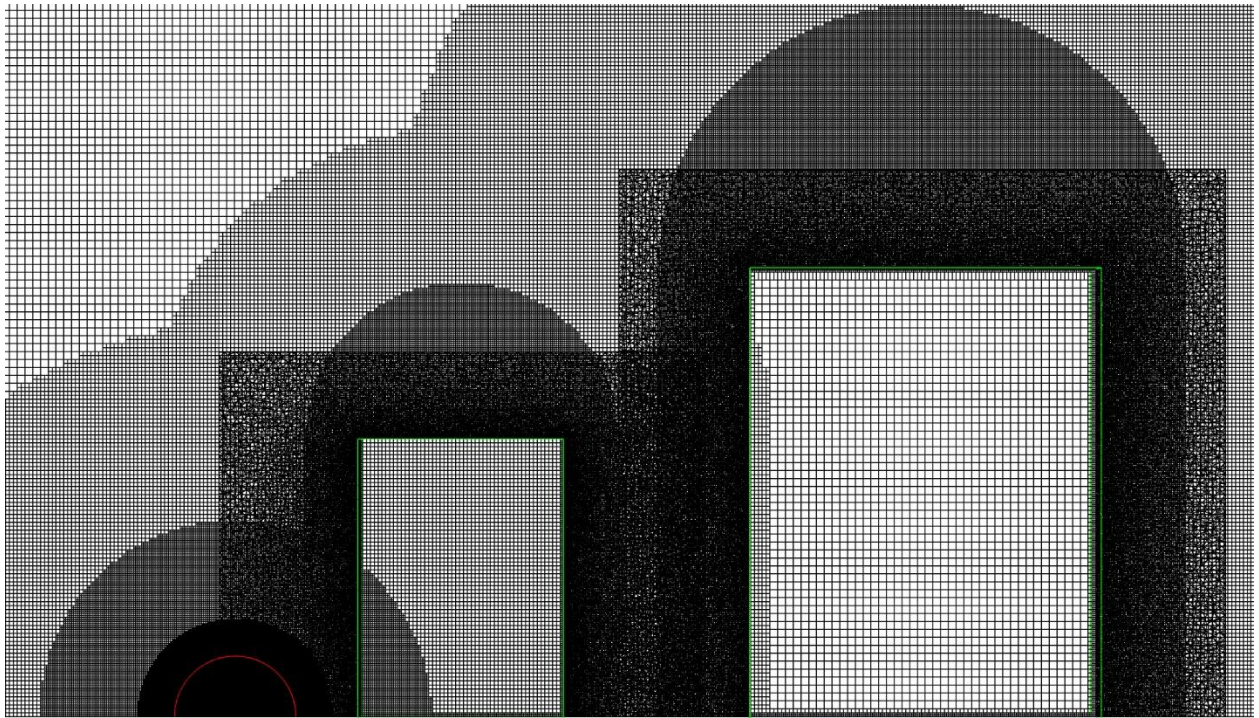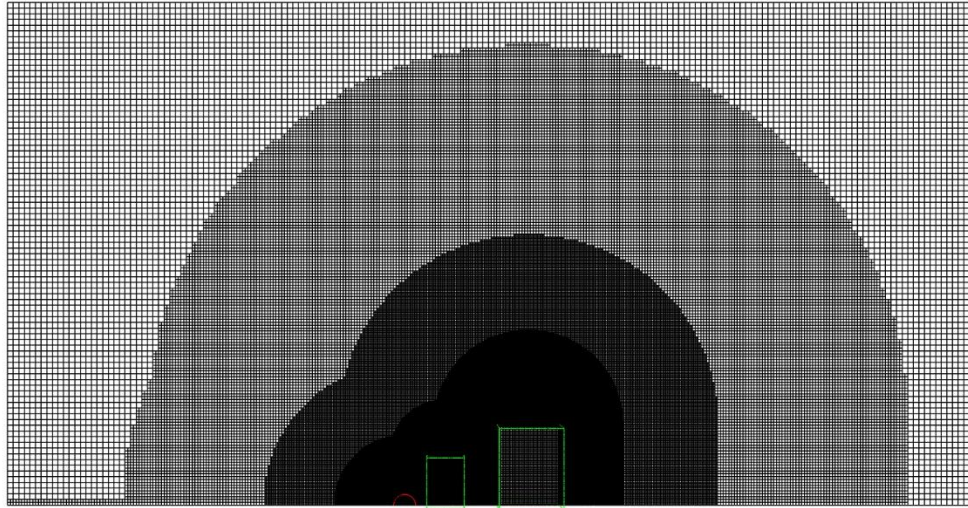
(b) Two-building overset mesh, full view (above) and close-up view (below)

Figure 3. Overset mesh refinement considering the existence of nearby buildings and a charge
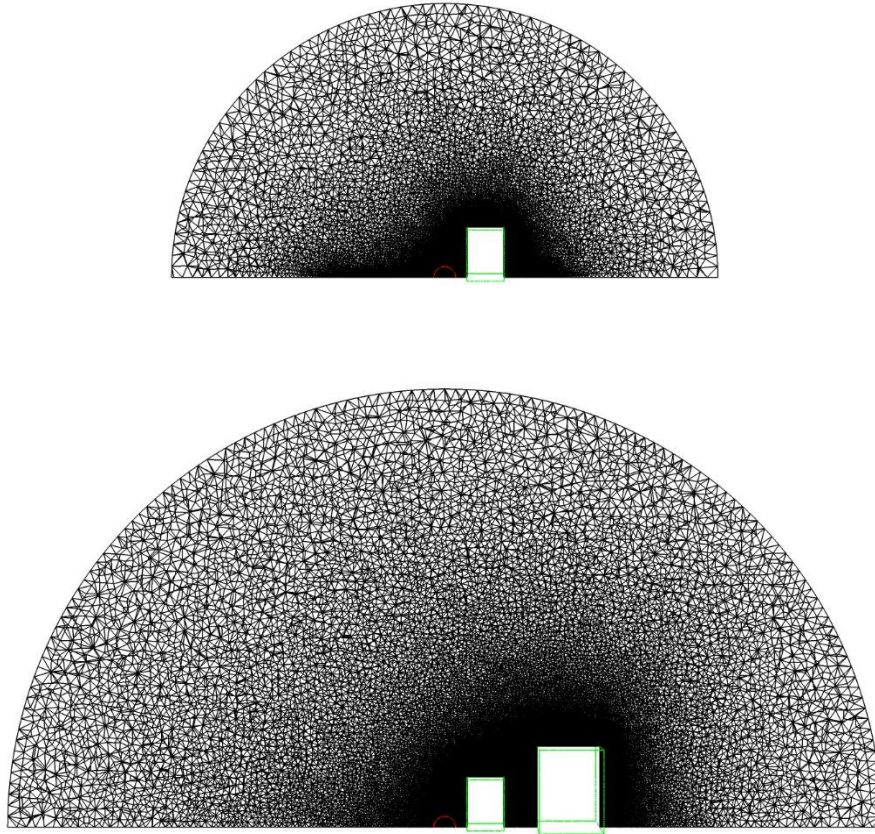
Figure 4. Single mesh, one-building case (above), two-building case (below)

5. AIR BLAST SIMULATIONS

Results predicted using *Loci/BLAST* are now compared to experimental data and simulations performed using *SHAMRC* [6]. A number of pressure transducers were placed on the structure to measure pressure histories. Pressure histories from the *Loci/BLAST* simulations at a few representative locations, as marked in Figure 1, were compared with the ERDC experimental data and the *SHAMRC* simulation results. Each *Loci/BLAST* simulation was initiated from an axisymmetric simulation for the detonation of the explosive material over a time interval of 0.0449 msec. The solution at the end of the axisymmetric simulation was then interpolated onto the three-dimensional mesh to provide initial conditions for the simulation. The baseline prescribed burn model was employed and the effects of secondary combustion

were not included. A far field boundary condition was specified on the domain outer boundary and a reflecting boundary condition was used on the ground and all building surfaces. In the overset mesh simulations, the outer boundary of each building component is an interface boundary, where variable interpolations were performed. Solution histories at the selected probe locations as indicated in Figure 1 were compared with the ERDC experimental data and the *SHAMRC* simulation results. Due to limitations on data distribution imposed by the Department of Defense, all presented data have been normalized with respect to a set of constant reference values chosen from the *Loci/BLAST* results. All simulations were performed on high-performance computing clusters located at the High Performance Computing Collaboratory (HPC²) at Mississippi State University.

In all cases, the hole cutting needed for the overset simulation was performed automatically as described in Section 4. Communication between the component meshes was performed using a cloud-of-points interpolation [1]. These two features allowed users to produce overset mesh simulations with only minimal input. For optimal robustness, the primitive variables of pressure, temperature, velocity, and mixture fraction were interpolated instead of the conservative variables. The JWL EoS for the explosive C4 was prescribed by assigning appropriate values to the parameters in the model. The prescribed burn model was used to simulate the propagation of the detonation front through the explosive material.

5.1   Air Blast for One-Building Configuration

Numerical solutions of pressure and impulse at selected probes were compared with the *SHAMRC* simulations and ERDC experimental data in Figures 5-8. At each probe, peak pressures and peak impulse predicted by *Loci/BLAST* were chosen to normalize the pressures and impulses, respectively. The physical time at each probe was normalized by the time when a negative gage pressure was first recorded in the simulation at that probe.

Since experimental data on the front wall of the small structure in the one-building test case (probe F marked in Figure 1) are not available, comparisons for the front wall (Figure 5) were made only between solutions of *Loci/BLAST* and *SHAMRC. SHAMRC* predicted a nearly 30% higher value and a 0.016 earlier scaled arrival time than *Loci/BLAST* for the peak pressure at probe F. Differences were observed between the *Loci/BLAST* solutions obtained on the overset mesh and single mesh in the peak pressures, a 20% lower first peak and a 15% lower second peak on overset mesh. This was due to the fact that blast front has extremely high gradients and velocities at this close standoff distance, and thus, simulation accuracy is highly mesh sensitive. Recalling the one-building overset mesh and single mesh addressed in section 4, resolutions were different between the two meshes since different surface spacings were used in the mesh generation. This could be the main reason that caused this moderate difference.

In terms of the calculated impulse, the difference between results on the two meshes is only 5 percent due to the fact that the peak pressure acting upon the front wall only for a very short period of time. Other than those differences, the predicted time histories of the pressure variation, especially the arrival time of peak pressures, are consistent between solutions obtained on the two meshes.
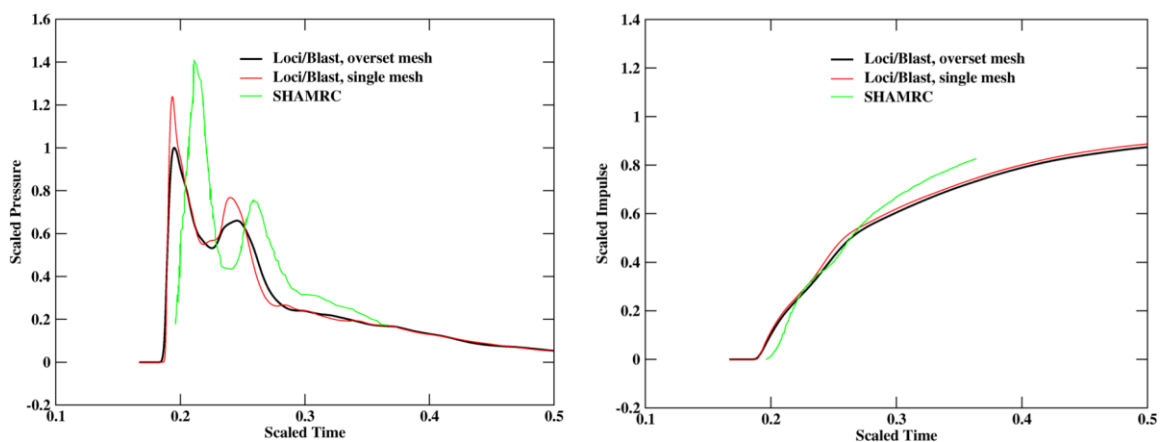
Figure 5. History of pressure (left) and impulse (right) at probe F, small building only

On the side wall (Figure 6), *Loci/BLAST* (overset mesh) overpredicted the first pressure peak by about 70% while *SHAMRC* overpredicted it by approximately 100%, as compared to the experimental data. The peak arrival time predicted by *Loci/BLAST* is earlier than the experimental measurements by 0.06 scaled time units, but the impulse histories are quite similar. The maximum difference in impulse between the overset mesh and single mesh is about 8%.

On the building top (Figure 7), all the numerical simulations captured the histories of pressure and impulse very well. But overpredictions of 25% by *Loci/BLAST* and 65% by *SHAMRC* were observed in the first pressure peak. Additionally, all simulations yielded a lagged arrival time for the second pressure peak, approximately 0.17 scaled time units. For data predicted on the building top, the overset mesh simulation and the single mesh simulation agreed very well.

Pressures on the back wall are shown in Figure 8. The predicted arrival time and impulse agree well with the experimental data. The predicted peak pressure is about 30% lower than the experimental data.

In this one-building simulation, good overall agreement was noted with the measured time-of-arrival and initial peak pressure at each of the gage locations. The arrival time of a secondary (reflected) peak lagged the measured data. This was a consequence of not including secondary combustion, or afterburn, in the model. Simulations using the overset mesh and the single mesh matched very well. A moderate difference was observed only in the peak value on the front wall, which captured an early stage blast wave.
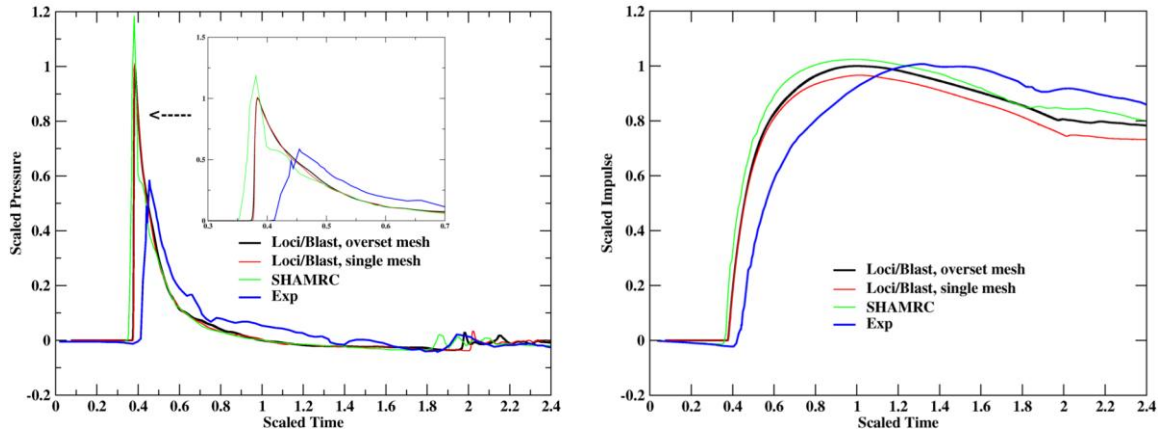
Figure 6. History of pressure (left) and impulse (right) of probe S, small building only
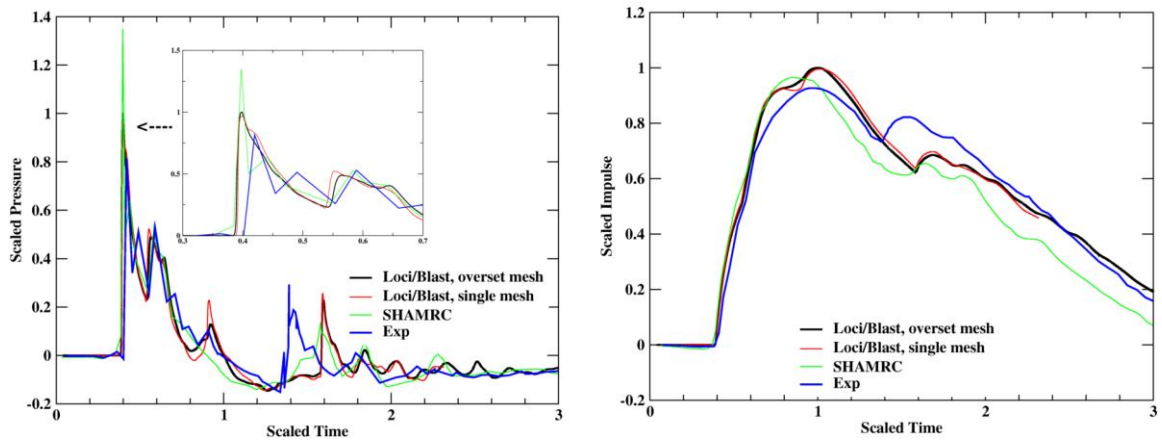
Figure 7. History of pressure (left) and impulse (right) of probe T, small building only
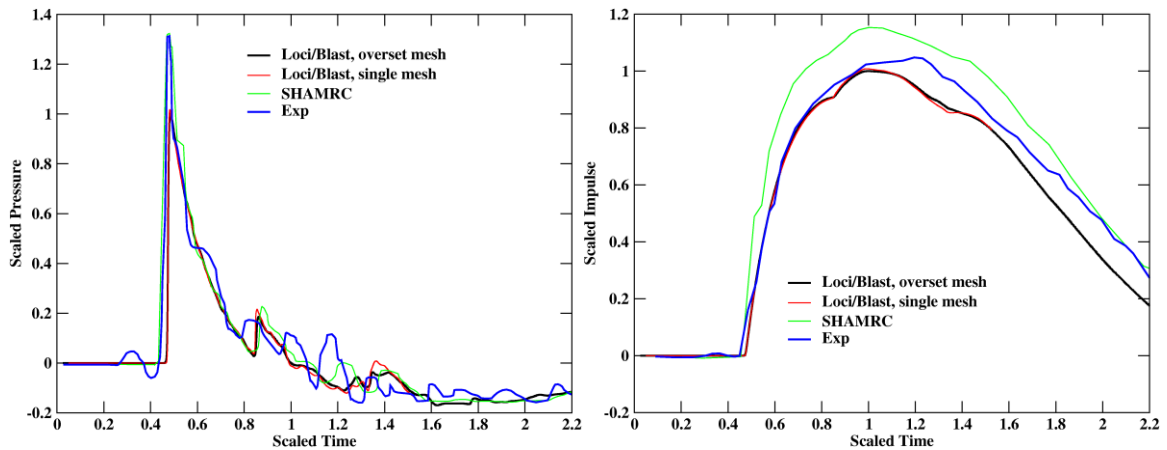
Figure 8. History of pressure (left) and impulse (right) of probe B, small building only

22

5.2 Air Blast for Two-Building Configuration

Assessing of the predictive capability of *Loci/BLAST* for blast loads on structures in proximity to neighboring structures was the primary motivation for the two building simulations. Pressure histories recorded at probes B and FF were compared with both ERDC experimental data and *SHAMRC* numerical results as shown in Figure 9. In order to compare results between the one-building and two-building cases for identifying the effect of the presence of the second building, solutions for two-building simulations were scaled by the same set of reference values used at probe B in the one-building case.

Probes B and FF (Figure 9) monitored pressure-time histories that showed two major pressure peaks for each probe and decaying pressures afterward. At probe B (Figure 10), the pressure history prior to the second peak matched the pressure observed in the one-building simulation. The first pressure peak at each probe was produced by the incident blast waves that diffracted from the top and sides of the small building (Figure 11 (a, b)).Waves reflecting between the two buildings contributed to the second peak pressure on each probe (Figure 11(c, d)). It is important to note that the second peak pressure of probe B was doubled as compared to the first peak. Pressure contours on the back wall of the small building (Figure 11 (a, c)) illustrated the much stronger second pulse, which revealed the fact that reflections off surrounding buildings can dramatically increase damage in an urban setting.

Large Building Front Wall

Small Building Back Wall
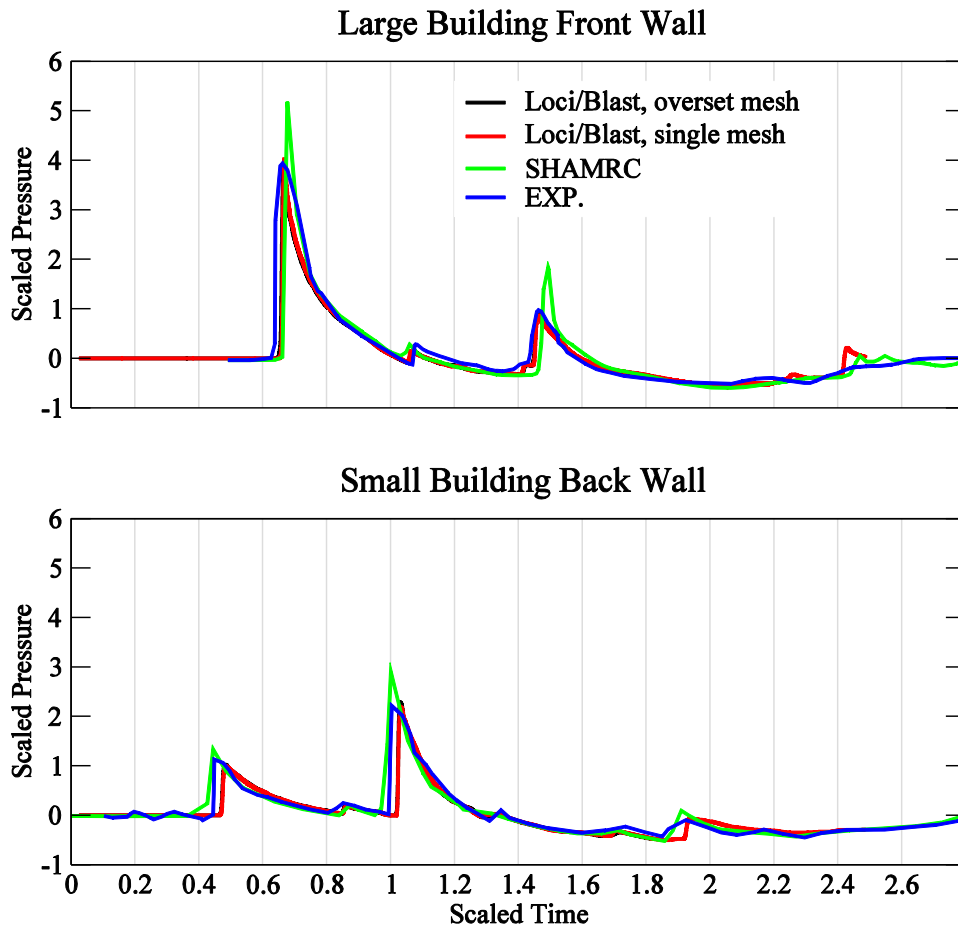
Figure 9. Alternating occurrence of pressure peaks due to wave reflections between large building (top) and small building (bottom)
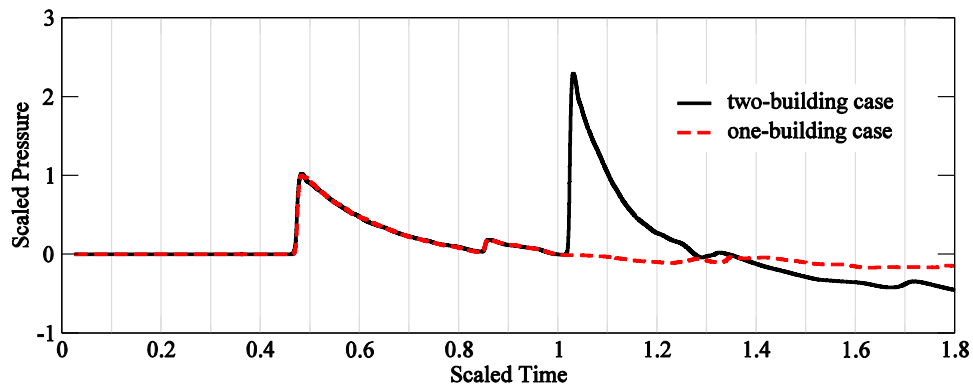
Figure 10. Predicted pressures for the back of the small structure.
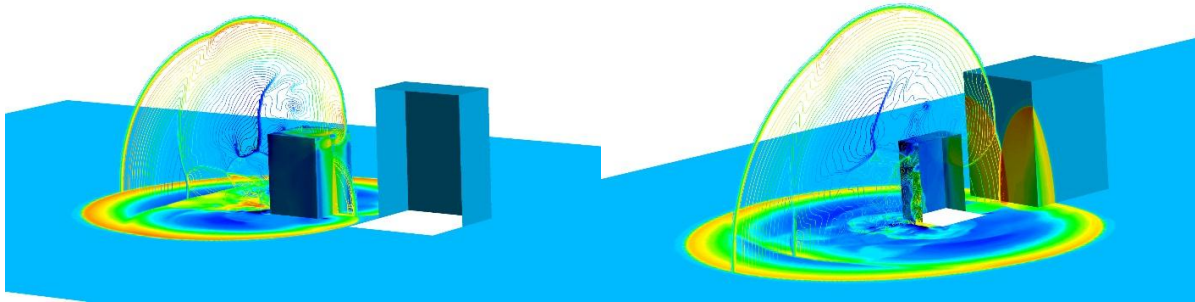
(a) First pressure peak at Probe B   **(b) First pressure peak at Probe FF**
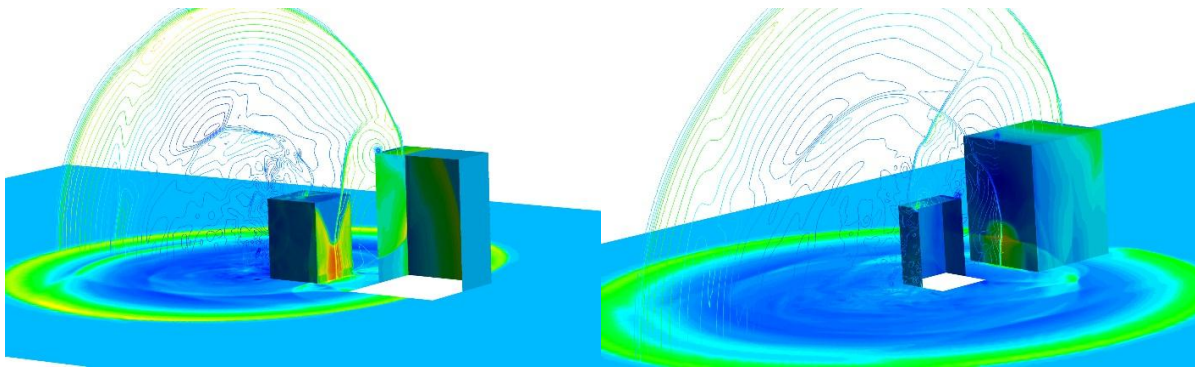
(c) Second pressure peak at Probe B   **(d) Second pressure peak at Probe FF**

Figure 11. Interactions of blast wave with structures under an urban setting

On the front wall of the large building, a more significant loading was expected compared to the back wall of the small building. Figure 12 shows three snapshots that illustrate the propagation and diffraction of the blast waves. The figure clearly shows that the blast wave was deflected around the edge of the small building and generated a Mach stem with a regional high pressure. The Mach stem approached the large building and merged around the center line of the front surface. Therefore, a very high pressure peak rapidly built up on the lower portion of the wall. Animations of the pressure contours revealed that another Mach stem approaching from the top of the small building struck the upper part of the large building at a later time. Accurate prediction of this time lag was considered essential for estimating the blast load and structural damage in an urban setting. The strength and motion of the peak pressure were clearly

illustrated through the pressure histories sampled at five locations along a vertical line on the

front wall centerline (Figure 13).
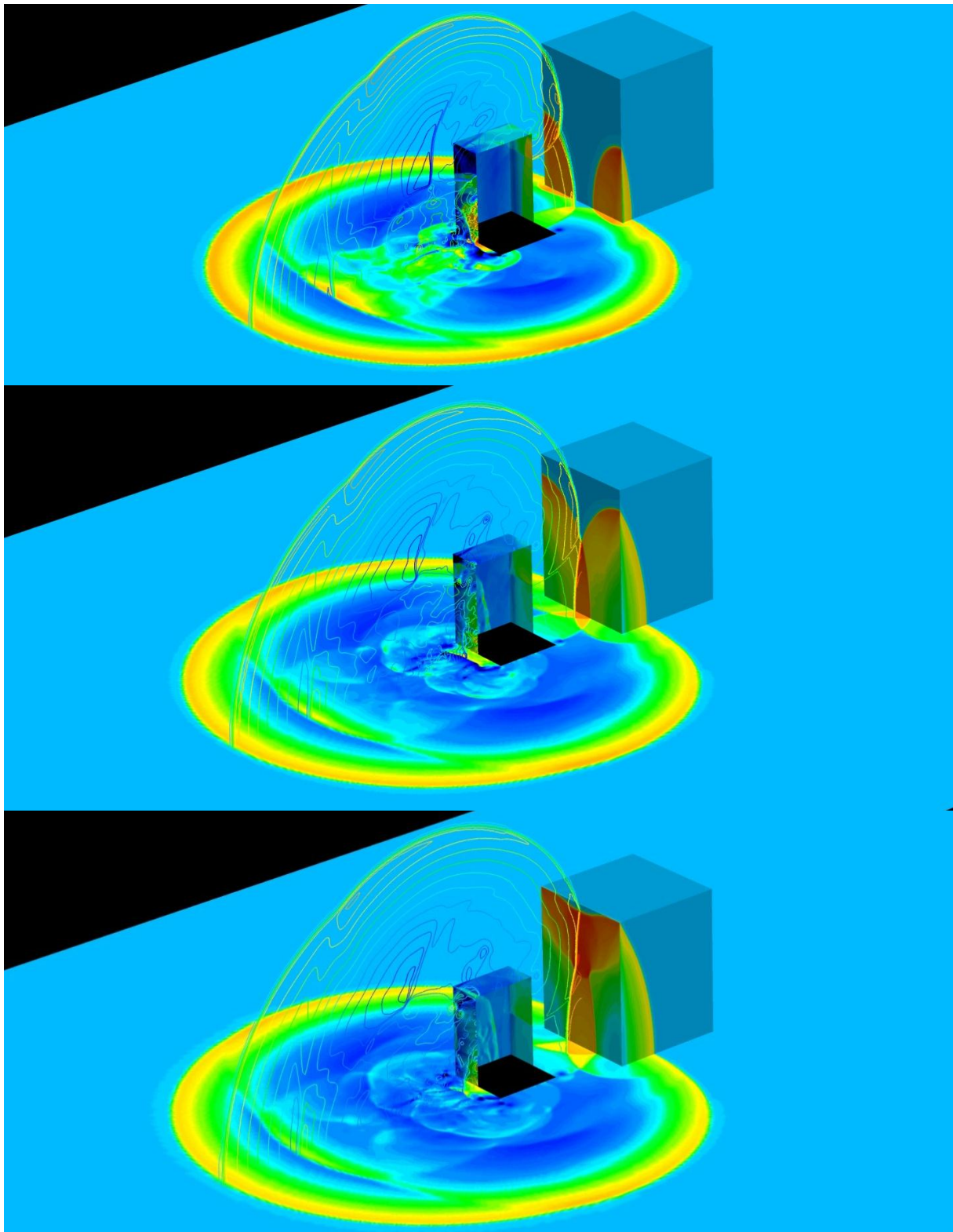
Figure 12. Time sequence with increment of 0.057 scaled time (from top to bottom) showing waves merging on the front wall of the large building
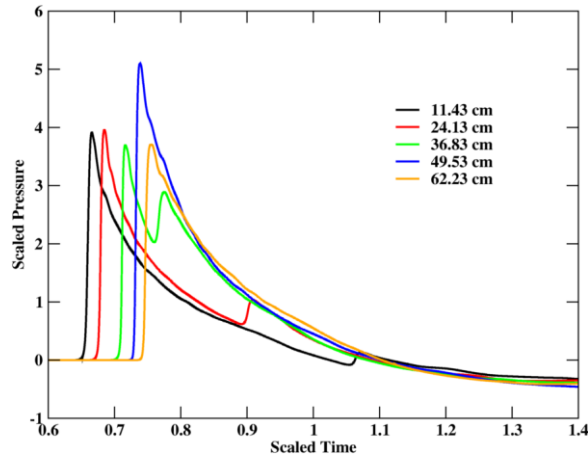
Figure 13. Pressure peak moving up (identified by height) along the front wall of the large building

In this two-building simulation, the *Loci/BLAST* simulation agreed very well with the ERDC experimental data. *Loci/BLAST* results demonstrated better agreement with the experimental data than did the SHAMRC results in terms of the pressure peaks. Very good agreement between solutions obtained on the overset and single meshes was also observed in the two-building simulation. This two-building simulation demonstrated the efficacy of this newly-developed blast analysis system for blast simulation in an urban environment. The wave propagation and evolution through multiple structures and the wave reflection and diffraction between structures were well captured with good agreement with the ERDC experimental data.

5.3 Computational Expense

Simulations were performed on two Linux clusters, IBM iDataPlex (2.8 GHz Intel Westmere; 3072 compute cores), and Sun X2200 M2 (2.6 GHz Opteron; 2048 compute cores). The computing costs are summarized in Table 1, in which each case was sampled when running on the IBM machine using 192 processors with data being saved frequently at every 5 µs simulation for animations. Computing time needed for a complete simulation was estimated based on the decay of the blast waves, i.e. when the overpressure on the back face of the small

structure decayed to ambient. The use of 192 processors is a limitation imposed by our HPC operating procedures and is not a limitation associated with *Loci/BLAST*. *Loci/CHEM*, the parent code of *Loci/BLAST*, has been demonstrated to scale effectively to thousands of processors and it is anticipated that *Loci/BLAST* would demonstrate similar scalability.

Table 1. Computational Expense

Case	Mesh Size (million cells)	Complete simulation time (hours)
1 building Single mesh	18.41	274
1 building Overset mesh	14.26	329
2 buildings Single mesh	47.44	480
2 buildings Overset mesh	62.27	667

6. SUMMARY AND CONCLUSIONS

Component-based geometry modeling and mesh generation were performed in a highly automated way to create overset meshes for blast simulations in an urban environment. *Loci/BLAST* simulations for the one-building case and the two-building case were conducted and validated against ERDC experimental data and exhibited good agreement. The *Loci/BLAST* results showed agreement that was better than that obtained using *SHAMRC*. The two-building simulation clearly captured the wave propagation, diffraction, merging, and reflection between the two buildings. Increased blast loading was predicted due to the presence of neighboring buildings, which can be critical for evaluating blast loadings, structural response, casualties and damages in an urban environment. These results indicate that overset meshing techniques are an effective tool that can be employed for urban blast simulations. The overset meshing paradigm allows for a component view of meshing such that ideal meshes can be constructed apriori for each component and assembled as needed, potentially by non-experts, in a seamless

28

fashion. Additionally, the overset meshing paradigm provides a mechanism to address more complex scenarios such as tracking debris where rigid or essentially rigid bodies are moving through the domain.

ACKNOWLEDGMENTS

REFERENCES

1. Thompson, D., Luke, E., Remotigue, M., Janus, M., Wang, X., Collins, E., Arnoldus, Q., Trcalek, M., Weed, R., Moore, C. and Tong, X., 2012. Multi-Fidelity Tools for Blast Analysis in Urban Environments. SERRI Report 90028-01, Oak Ridge National Laboratory, Aug 2012.

2. Thompson, D., Janus, J.M., Luke, E., More, E., Remotigue, M., Tong, X.L., Weed, R., and Ivancic, P. 2012. Enhanced Simulation of Blast-Vehicle Interactions using *Loci/BLAST* and LS-DYNA. Final Report for SimBRS WD 0034, Contract No. W56HZV-08-C-0236.

3. Thompson, D., Luke, E., Newman III, J.C., Janus, M., Blades, E., Tong, X., and Moore, C., 2010. Development of a Strategy for Simulating Blast-vehicle Interactions. TACOM/TARDEC Report 21200RC. U.S. Army Tank Automotive Research Development and Engineering Center, Warren, MI.

4. Ivancic, P., Janus, J.M., Luke, E., Thompson, D., Weed, R. and Kang, J., 2014. A Conformal, Fully-Conservative Approach for Predicting Blast Effects on Ground Vehicles. NATO Paper MP-AVT-221-05, Design and Protection Technologies for Land and Amphibious NATO Vehicles, Copenhagen, DK, Apr 7-9, 2014.

5. Meakin, R., 1999. Composite overset structured grids. The Handbook of Grid Generation. 11-1. eds. Thompson, J., Soni, B. and Weatherill, N., CRC Press.

6. Crepeau, J. 1998. SHAMRC Second-Order Hydrodynamic Automatic Mesh Refinement Code, Vol. 2: User's Manual. Applied Research Associates, Inc., Albuquerque, NM.

7. Fairlie, G.E., 1997. Efficient Analysis of High Explosive Air Blast in Complex Urban Geometries Using the AUTODYN-2D & 3D Hydrocodes, Analytical Experiments and Methods. 15th International Symposium on Military Application of Blast and Shock, MABS 15, Sep. 1997, Banff, Canada.

8. Wrobel, K., Schultz, P. and Crawford, D., 2006. An Atmospheric Blast/Thermal Model for the Formation of High-Latitude Pedestal Craters. Meteoritics & Planetary Science, 41(10):1539-1550.

9. Jiang, D., Qi, C., Ma, Z., Raju, B., Bryzik, W., 2007. Innovative Composite Design for Blast Protection. SAE World Congress and Exhibition, 2007-01-0483.

10. Alia, A. and Souli, M., 2006. High Explosive Simulation Using Multi-Material Formulations. Applied Thermal Engineering 2006; 26(10):1032-42.

11. Chafi, M.S., Karami, G. and Ziejewski, M. 2009. Numerical Analysis of Blast-Induced Wave Propagation Using FSI and ALE Multi-Material Formulations. International Journal of Impact Engineering, 36(10-11):1269-1275.

12. McGlaun, J.M., Thompson, S.L. and Elrick, M.G., 1990. CTH: a Three-Dimensional Shock Wave Physics Code. International Journal of Impact Engineering, 99:351-360.

13. Crepeau, J., Needham, C. and Hikida, S., 2001. SHAMRC Second-Order Hydrodynamic Automatic Mesh Refinement Code, vol.1: Methodology. Applied Research Associates, Albuqurque, NM.

14. Luo, H., Baum, J.D., Lohner, R. and Cabello, J., 1993. Adaptive Edge-Based Finite Element Schemes for the Euler and Navier-Stokes Equations. AIAA-93-0336.

15. Baum, J.D., Luo, H. and Lohner, R., 1995. Numerical Simulation of Blast in the World Trade Center. AIAA Paper 95-0085.

16. Rice, D.L., Baum J.D., Togashi, F., Löhner, R. and Amini, A., 2008. First-Principles Blast Diffraction Simulations on a Notebook: Accuracy, Resolution and Turn-Around Issues. Proceedings of the 20th International Symposium on Military Aspects of Blast and Shock, MABS 20, Sep. 2008, Oslo, Norway.

17. Gittings, M.L., Weaver, R.P., Clover, M., Betlach, T. and Byrne, N., 2006. The Rage Radiation- Hydrodynamic Code. Los Alamos National Laboratory Report LA-UR-06-0027. Los Alamos, NM.

18. Schlamp, R.J., Hassig, P.J., Nguyen, C.T., Hatfield, D.W. and Hookham. P.A., 1995. MAZ User's Manual. Technical Report DNA001-91-C-0153. Defense Nuclear Agency, Washington, DC.

19. Ripley, R.C., Cloney, C., Donahu, L., Frost, D.L. and Zhang, F., 2010. Enhanced Loading Due to Reflected Heterogeneous Blast. Proceedings of the 21st International Symposium on Military Aspects of Blast and Shock, MABS 21, Oct. 2010, Jerusalem, Israel.

20. Century Dynamics. 2003. AUTODYN 2-d & 3-d User's Manual.

21. Cowler, M.S., Quan, X. and Fairlie, G.E., 2004. A Computational Approach to Assessing Blast Damage in Urban Centers Using AUTODYN. Paper PVP2004-3044, ASME/JSME 2004 Pressure and Piping Conference.

22. Nichols, A., 2007. User Manual for ALE3D: An Arbitrary Lagrangian-Eulerian 3D Code System. Technical Report, UCRL-MA-152204 Rev. 6. LLNL, Livermore, CA.

23. Halquist, J.O., 2006. LS-DYNA Theory Manual. Livermore Software Technology Corporation, Livermore, CA.

24. Hyde, D.W., 1991. User's Guide for Microcomputer Programs CONWEP and FUNPRO, Applications of TM5-855-1. Instructional Report SL-88-1. U. S. Army Engineering Research and Development Center, Vicksburg, MS.

25. Bessette, G., Vaughn,C., Bell, R., Yarrington, P. and Attaway, S., 2003. ZAPOTEC: A Coupled Eulerian-Lagrangian Computer Code, Methodology and User Manual, Version 1.0. Sandia Technical Report. Sandia National Laboratories, Albuquerque, NM.

26. McKeown, R., Dengel, O., Harris, G. and Diekhoff. H.J., 2004. Development and Evaluation of DYSMAS Hydrocode for Predicting Underwater Explosion Effects, Executive Summary. Vol. 1 IHTR 2492. Naval Surface Warfare Center, Indian Head, MD.

27. Luke, E. and Cinnella, P., 2007. Numerical Simulations of Mixtures of Fluids Using Upwind Algorithms. Computers and Fluids 36:1547-1566.

28. Lee, E and Tarver, C., 1980. Phenomenological Model of Shock Initiation in Heterogeneous Explosives. Physics of Fluids 23:2362–2372.

29. Veluri, S., Roy, C.J. and Luke, E., 2010. Comprehensive Code Verification for an Unstructured Finite Volume CFD Code. 48th AIAA Aerospace Sciences Meeting, January 4-7, 2010, Orlando FL, AIAA paper #AIAA 2010-127.

30. Li, Y.-H., 1972. Equation of State for Water and Sea Water. Journal of Geophysical Research, 72(10):2665-2678.

31. Fiserova, D., 2006. Numerical analysis of buried mine explosions with emphasis on effect of soil properties on loading. PhD thesis, Cranfield University.

32. Einfeldt, B., 1988. On Godunov-Type Methods for Gas Dynamics. SIAM Journal on Numerical Analysis, Vol. 25(2):294-318.

33. Barth, T.J., and Jespersen, D.C., 1989. The Design and Application of Upwind Schemes on Unstructured Meshes. AIAA-89-0366.

34. Shu C-W and Osher S., 1988. Efficient Implementation of Essentially Non-Oscillatory Shock-Capturing Schemes. Journal of Computational Physics, Vol. 77(2):439-471.

35. Chalasani, S., Senguttuvan, V., Thompson, D. and Luke, E., 2008. On the Use of General Elements in Fluid Dynamics Simulations. Communications in Numerical Methods in Engineering, 24(6):435-448.

36. Togashi, F., Nakahashi, K., Ito, Y., Iwamiya, T. and Shimbo, Y., 2001. Flow Simulation of NAL Experimental Supersonic Airplane/booster Separation Using Overset Unstructured Grids. Computers and Fluids. 30:673–688.